

Brain MR Perfusion-Weighted Imaging With Alternate Ascending/Descending Directional Navigation

Sung-Hong Park* and Timothy Q. Duong†

In this study, a new arterial spin labeling technique that requires no separate spin preparation pulse was developed. Sequential two-dimensional slices were acquired in ascending and descending orders by turns using balanced steady state free precession for pair-wise subtraction. Simulation studies showed this new technique, alternate ascending/descending directional navigation (ALADDIN), has high sensitivity to both slow- (1–10 cm/sec) and fast-moving (>10 cm/sec) blood because of the presence of multiple labeling planes proximal to imaging planes and sensitivity of balanced steady state free precession to initial magnetization differences. ALADDIN provided high-resolution multislice perfusion-weighted images in ~3 min. About 80–90% of signals in a slice were ascribed to spins saturated in the four prior slices. Three to five edge slices on each side of imaging group were affected by transient magnetization transfer effects and incomplete T_1 recovery between successive acquisitions. ALADDIN signals were dependent on many imaging parameters, implying room for improvement. Sagittal and coronal ALADDIN images demonstrated perfusion direction in gray matter regions was mostly from center to lateral, anterior, or posterior, whereas that in some white matter regions was reversed. ALADDIN is likely useful for many studies requiring perfusion-weighted imaging with short scan time, insensitivity to arterial transit time, directional information, high resolution, and/or wide coverage. Magn Reson Med 65:1578–1591, 2011. ©2010 Wiley-Liss, Inc.

Key words: arterial spin labeling; perfusion-weighted imaging; perfusion directionality; white matter perfusion; balanced steady state free precession; alternate ascending/descending directional navigation

Blood perfusion has been noninvasively imaged with arterial spin labeling (ASL). All ASL methods use a separate spin preparation for labeling of arterial blood in advance to data readout for pair-wise subtraction. Improvement of ASL techniques has been mostly about improvement of spin preparation methods, such as pulsed ASL (PASL) (1–5), continuous ASL (6–11), and pseudo-continuous (or pulsed-continuous) ASL (pCASL) (12–14). Despite these improvements and the noninvasive nature, ASL has not been routinely used in clinical

applications because of its intrinsic limitations. One is relatively low percent signal change (PSC) between label and control images that require many averages to achieve reasonable signal-to-noise ratio (SNR) even with relatively low resolution. Another is the narrow time window permitted for the perfusion contrast that limits baseline image qualities. The third is sensitivity to tissues with heterogeneous arterial transit times. Perfusion in tissues with longer arterial transit time is likely underestimated in ASL due to enhanced T_1 recovery of labeled arterial spins. The fourth is that perfusion directionality is not easily assessable with multiple slices, as labeling direction cannot be easily changed.

The aforementioned limitations may be overcome, if we can put the spin labeling plane right next to the imaging planes while maintaining the multislice capability. This may be achieved by acquiring multiple slices in the sequential order but in two different directions of ascending and descending, with no separate spin preparation. For the axial imaging case, slices sequentially acquired in the direction away from the heart (“ascending” in this article) work as labeling and those in the direction toward the heart (“descending” in this article) work as a control. In this new perfusion-weighted imaging technique, alternate ascending/descending directional navigation (ALADDIN), spin preparation and imaging parts are not separated: imaging one plane works simultaneously as spin preparation for the next imaging planes. Balanced steady state free precession (bSSFP) (15) may be a good choice for ALADDIN because of its high flip angle, high temporal resolution, and good sensitivity to the initial magnetization differences (16,17). In this sense, bSSFP has also been used for perfusion-weighted imaging with the conventional labeling methods (16–18).

The anticipated problems with the ALADDIN approach are transient magnetization transfer (MT) effects and incomplete T_1 recovery between successive ascending/descending acquisitions in edge slices, MT asymmetry, field inhomogeneity, and gradient imperfection (9). The problems in the edge slices may be handled by discarding them. MT asymmetry, field inhomogeneity, and gradient imperfection may be resolved by averaging over alternating slice gradient polarities (9). As imaging a slice works simultaneously as labeling the following slices, different scan direction (e.g., axial, sagittal, and coronal) would provide differential perfusion information because of changes in the labeling direction. In this article, feasibility of this new technique, ALADDIN, was tested for brain perfusion imaging with various scan conditions using bSSFP, and the results were compared with a conventional PASL method.

Research Imaging Institute and Department of Radiology, University of Texas Health Science Center at San Antonio, San Antonio, Texas, USA.

Current affiliation for Dr. Park: Department of Radiology, School of Medicine, University of Pittsburgh, Pittsburgh, Pennsylvania, USA.

†This article was published online 21 September 2010. Timothy Q. Duong was subsequently acknowledged as a coauthor. This notice is included in the print and online versions to indicate that both have been corrected 18 May 2011.

*Correspondence to: Sung-Hong Park, Ph.D. 200 Lothrop Street PUH-B864.2, Pittsburgh, PA 15213. E-mail: parks@upmc.edu

Received 8 February 2010; revised 22 June 2010; accepted 29 June 2010.

DOI 10.1002/mrm.22580

Published online 21 September 2010 in Wiley Online Library (wileyonlinelibrary.com).

© 2010 Wiley-Liss, Inc.

1578

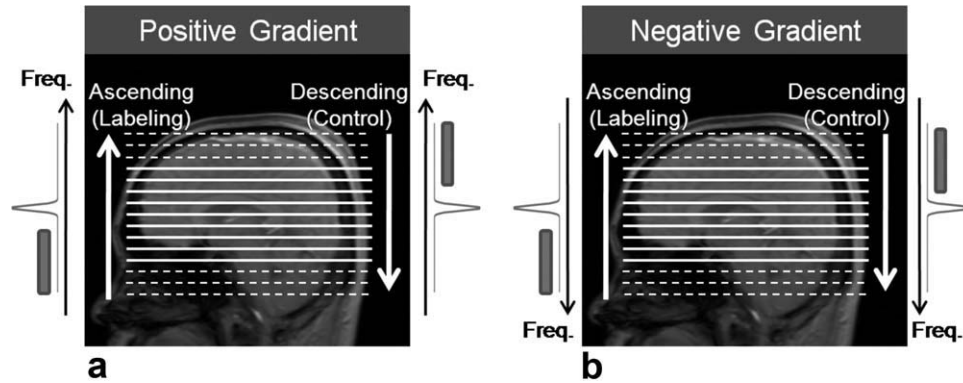


FIG. 1. Schematic diagrams demonstrating ALADDIN method. Slices sequentially acquired in the direction away from the heart (“ascending”) work as labeling and those in the direction toward the heart (“descending”) work as a control. The ascending and descending acquisitions are also alternated between the positive (a) and negative (b) slice-select gradients. No separate spin labeling part exists in ALADDIN. The small boxes above the frequency spectrum represent the locations of interslice MT effects. Broken lines represent dummy slices, where MT effects are not in the steady state and longitudinal magnetizations are not fully recovered between successive acquisitions.

THEORY

An image from sequentially acquired two-dimensional (2D) multiple slices is slightly different from the image acquired as a single 2D slice because of interactions between slices. Signals in a slice can be affected by prior slices in three different ways: interslice flow effects (19), MT effects (20–22), and crosstalk effects due to imperfect excitation profile of radiofrequency (RF) pulses. The goal of this study is to maximize the interslice flow effects (hence, perfusion effects) and minimize the MT and crosstalk effects.

It is assumed that flow spins move through 2D slices with a constant velocity in a blood vessel (“transport” stage) and then perfuse after moving into capillaries in the slice of interest (“perfusion” stage). For blood vessels not perpendicular to the 2D slices, the velocity component along the axis perpendicular to the 2D slices determines the characteristics of labeling; hence, it is denoted by simply “velocity” throughout this article. When acquisition time of one slice $\cong 800$ msec, slice thickness = 5 mm, and gap = 7 mm (as used in most studies in this article), flow spins with velocity >1.5 cm/sec ($\cong 12$ mm/800 msec) that experienced RF excitations in one slice would not experience further RF excitations in the following slices until they perfuse in the slice of interest. Flow spins with velocity ≤ 1.5 cm/sec may experience labeling in more than one slice, but this cumulative labeling effect is neglected for simplicity.

Out-of-slice flow spins that have experienced RF excitations in one slice have different initial magnetizations compared with static spins in the following slices. Depending on the flow direction, these flow spins in sequential 2D imaging will contribute to the slice of interest in a completely different manner between ascending and descending acquisitions (ALADDIN). The minimum velocity required for flow spins to contribute to the slice of interest as perfusion signals (rather than inflow signals) is interslice gap divided by acquisition time of one slice (~ 800 msec), i.e., ~ 0.9 , 0.5 , and 0.1 cm/sec for the gap value of 7, 4, and 1 mm, respectively. This indicates that ALADDIN may have high sensitivity to slow-moving spins of velocity 1–10 cm/sec. During the transport stage,

magnetizations of out-of-slice flow spins are changed (labeled) in a manner dependent on the number and start point of RF excitations in the labeling slice. During the perfusion stage, differences in the initial magnetizations between static and labeled flow spins can be sensitized by bSSFP even after many RF excitations (16,17). Summation of all the out-of-slice flow spins from multiple labeling planes and multiple velocity components may provide high perfusion signals in ALADDIN. Computer simulations were performed to gain insight into spin evolution of flow spins with various velocities across 2D bSSFP imaging slices.

The conventional MT effects in *in vivo* brains are not symmetric around the water resonance frequency (9,23,24) and hence may not be identical between ascending and descending acquisitions. To further suppress these MT asymmetry effects, the sequential 2D slices can be acquired in four different methods (rather than two) with combination of two different acquisition orders (ascending and descending) and two different slice-select gradients (positive and negative) (Fig. 1), similar to the method used in a previous ASL study (9). In the view point of MT asymmetry, the two datasets acquired with ascending order and positive gradient (Pos_Asc, left side of Fig. 1a) and with descending order and negative gradient (Neg_Des, right side of Fig. 1b) are affected by MT effects from frequencies lower than the water resonance frequency. Similarly, the two datasets acquired with ascending order and negative gradient (Neg_Asc, left side of Fig. 1b) and with descending order and positive gradient (Pos_Des, right side of Fig. 1a) are affected by MT effects from frequencies higher than the water resonance frequency. Therefore, to suppress the MT asymmetry effects, the perfusion-weighted images should be calculated as subtraction between Pos_Asc and Neg_Des or between Neg_Asc and Pos_Des. Eventually, as demonstrated later in this study, combination of the four datasets would provide better results by further suppressing magnetic field inhomogeneity and gradient imperfections.

Crosstalk effects in sequential 2D multiple slices are relatively small compared with those in 2D multislice

images interleaved along phase-encoding (PE) dimension because of T_1 recovery but still may be comparable with perfusion signals. A relatively big gap (140% of the slice thickness) was used to avoid the potential crosstalk effects in most studies in this article. Also gap-dependent studies were performed in both human brains and uniform phantoms to see the signal enhancement and crosstalk effects. To investigate the influence of changing number of labeling planes on the ALADDIN signals, a series of ALADDIN scans were performed with varying numbers of slices. The sensitivity of ALADDIN to flow directions (hence to perfusion directions) was tested with ALADDIN scans performed along sagittal and coronal directions. As the distance between labeling and imaging planes is short in ALADDIN, flow spins from vein and cerebrospinal fluid (CSF) might contribute to ALADDIN signals and hence were also investigated and discussed.

MATERIALS AND METHODS

Data Acquisitions

All experiments were performed on a 3T whole-body scanner (Siemens Medical Solutions, Erlangen, Germany) with a body-coil transmission and a 12-element head matrix coil reception. Totally eight normal volunteers were scanned in this study approved by the Institutional Review Board. Foam padding and plastic clamps were used to minimize subject head motion. Voxel-localized shimming was performed within a region covering whole brain with a vendor-supplied second-order shim module based on a three-dimensional phase image, which was repeated three times to improve magnetic field homogeneity. To get perfusion images, 2D bSSFP images were acquired in two different ways: one in sequentially ascending order and the other in sequentially descending order (Fig. 1). To compensate for MT asymmetry, field inhomogeneity, and gradient imperfection, the images with the ascending and descending orders were acquired with positive slice-select gradient first and then with negative slice-select gradient and these four acquisitions were repeated for average. Default imaging parameters to get a set of perfusion images were pulse repetition time (TR)/echo time = 4/2 msec, flip angle = 50° , matrix size = 128×96 , field of view = $240 \times 180 \text{ mm}^2$, thickness = 5 mm, gap = 7 mm (140% of thickness), number of slices = 15 (including dummy slices on each side), acquisition bandwidth = 575 Hz/pixel, scan direction = axial, PE order = linear, PE direction = left–right, delay time between repetitions $\cong 1$ sec, and total scan time = 3 min. No flow compensation gradient was used. Initial 10 PE steps were used as dummy scans, during which the flip angle linearly increased from 0° to 50° . The excitation RF pulse was a Hanning-windowed sinc pulse with two side lobes, 1 msec duration, and 1.6 kHz bandwidth. These scan parameters were maintained for most ALADDIN acquisitions unless specified otherwise.

For six subjects, three ALADDIN datasets were acquired with phase oversampling of 0, 100, and 200% and corresponding number of repetitions of 24, 12, and 8, respectively, to modulate the labeling efficiency. Scan time for each of the three datasets was almost the same at ~ 3 min. The acquisition time for one volume (15 slices)

per repetition was 6.4, 12.7, and 19.0 sec for phase oversampling of 0, 100, and 200%, respectively. Two more ALADDIN datasets were acquired with number of slices = 9 and 3 to investigate the effects of various numbers of labeling planes, and another two ALADDIN datasets with gap = 4 and 1 mm (80% and 20% of thickness) to see the effects of selecting different flow velocities. Finally, two additional datasets were acquired along sagittal and coronal directions with number of slices = 19 to cover wider regions for investigation of sensitivity of ALADDIN to perfusion direction. The coronal images were acquired with the default condition, whereas the sagittal images were acquired with matrix size = 128×128 and field of view = $240 \times 240 \text{ mm}^2$. Total scan time for the sagittal and coronal scans were 4.6 and 3.6 min, respectively. These studies dependent on number of slices, gap, and scan direction were performed with phase oversampling of 0% (number of repetitions = 24) for three subjects and with phase oversampling of 100% (number of repetitions = 12) for the remaining three subjects. The scan parameters for the axial ALADDIN experiments are summarized in Table 1. Note that most middle slices were acquired with an interval between successive (ascending and descending) acquisitions longer than three times blood T_1 (~ 5 sec; including the delay time of ~ 1 sec between repetitions) and hence would be free of incomplete T_1 recovery, except five, three, and two edge slices on each side when phase oversampling was 0, 100, and 200%, respectively.

For comparison reference to ALADDIN, additional perfusion images were acquired with a PASL sequence (5) for the six subjects. Thickness, gap, and scan direction were the same as those from the default scan condition of ALADDIN. Other scan parameters were TR = 4 sec, echo time = 30 msec, field of view = $240 \times 240 \text{ mm}^2$, matrix = 64×64 , PE direction = anterior–posterior, number of slices = 7, partial Fourier = 75%, number of repetitions = 46, and total scan time = 3.1 min. Spin labeling was performed in a 10-cm labeling region with 1 cm gap to the proximal edge of the imaging region, inversion time (TI), $TI_1 = 700$ msec, $TI_2 = 1800$ msec, and $TI_{1s} = 1600$ msec (5).

In a separate study for five subjects, ALADDIN was performed with centric PE order and with three interslice post imaging delay (PID) times of 0, 500, and 1000 msec in comparison with linear PE order, to see the effects of changing the postlabeling delay time. Three out of the five subjects attended the aforementioned study as well. Most scan parameters were similar to the aforementioned default condition, except number of slices = 13, gap = 5 mm (100% of slice thickness), and phase oversampling = 200%. To improve signal stability for the centric PE order, additional 40 dummy PE steps with the constant flip angle (50°) were employed right after the 10 dummy PE steps with the linearly increasing flip angle. Note that the effective PID increased by 200 msec (200, 700, and 1200 msec) when the total 50 dummy PE steps were taken into account.

To investigate the slice crosstalk effects, the aforementioned gap-dependent studies were also performed for two uniform phantoms with no MT effects: one with T_1 and T_2 of 110 and 75 msec, respectively, and the other

Table 1
Scan Parameters Used in Various Axial ALADDIN Experiments

Experiment	PHOS (%)	No. PE steps	No. slices	NEX	Gap (%)	PID (msec)	PE order	<i>N</i>
Labeling efficiency (PHOS)	0	96	15	12	140	40	Linear	6
	100	192	15	6	140	40	Linear	6
	200	288	15	4	140	40	Linear	6
No. of labeling planes with PHOS 0% (No. slices)	0	96	15	12	140	40	Linear	3
	0	96	9	12	140	40	Linear	3
	0	96	3	12	140	40	Linear	3
No. of labeling planes with PHOS 100% (No. slices)	100	192	15	6	140	40	Linear	3
	100	192	9	6	140	40	Linear	3
	100	192	3	6	140	40	Linear	3
Flow velocities with PHOS 0% (Gap)	0	96	15	12	140	40	Linear	3
	0	96	15	12	80	40	Linear	3
	0	96	15	12	20	40	Linear	3
Flow velocities with PHOS 100% (Gap)	100	192	15	6	140	40	Linear	3
	100	192	15	6	80	40	Linear	3
	100	192	15	6	20	40	Linear	3
Postlabeling delay with centric PE order (PID)	200	288	13	4	100	200	Centric	3
	200	288	13	4	100	700	Centric	3
	200	288	13	4	100	1200	Centric	3

PHOS represent phase oversampling. NEX represents number of excitations (averages) for pair-wise subtraction. PID represents effective postimaging delay time. The parentheses in the leftmost column represent the variable used in each experiment.

with T_1 and T_2 of 4000 and 500 msec, respectively. The phantom with longer T_1 was also used to measure the excitation profile of the RF pulse by acquiring two consecutive single-slice bSSFP images along sagittal and axial directions with higher in-plane resolution of $0.8 \times 0.8 \text{ mm}^2$.

Reconstruction, Data Analysis, and Simulations

There were four different datasets repeatedly acquired for average in ALADDIN. Motion correction (25) was applied to each of the four datasets separately, which provided better results than those with the motion correction applied to the whole four datasets. The datasets from the ascending and descending orders were separately averaged for subtraction. ALADDIN perfusion-weighted images were then reconstructed as PSC between ascending and descending acquisitions, unless specified otherwise. Subtraction polarity determined the perfusion direction in ALADDIN; hence, ascending and descending acquisitions had interchangeable roles as labeling and control, depending on the perfusion direction of interest. Acquisition order in the same direction as perfusion direction was set to labeling and that in the opposite direction to the perfusion direction was set to control. Subtraction was then performed as “control–labeling”. Perfusion images from PASL were also reconstructed as PSC with the vendor-supplied motion correction algorithm applied to the whole control and label images together. Only positive values were displayed in images, whereas all positive, zero, and negative values were used in quantifications with no rectification. For comparison with ALADDIN perfusion-weighted images, ALADDIN MT asymmetry signals were calculated by performing subtraction between ascending acquisitions (Neg_Asc–Pos_Asc) and between descending acquisitions (Pos_Des–Neg_Des) and then by averaging the two

subtraction images, where blood perfusion signals were suppressed.

For the measurement of PSC and SNR, whole gray matter (GM) and white matter (WM) regions and a noise region outside brain were manually segmented in the center slice of baseline images. PSC was measured from the aforementioned PSC images, and SNR from the subtraction images between ascending and descending acquisitions. Note that the polarity of PSC and SNR represented perfusion direction; hence, heterogeneity in perfusion directions might be reflected in the SD of PSC and SNR measured within a region of interest. To understand the heterogeneity in perfusion directions better, both mean and SD of PSC and SNR within each of GM and WM regions were quantified across subjects.

To gain insight into the evolution of flow spins across 2D bSSFP slices, numerical simulations were performed based on Bloch equations (26), under the default scan condition and number of PE steps = 192, T_1 and T_2 of blood = 1550 and 250 msec (13), respectively, and frequency offset = 0 Hz. Flow spins were assumed to experience RF excitations in an initial slice, move through the slices with velocity 30, 20, 10, 5, 2.6, and 1.7 cm/sec, and then to perfuse in the slice of interest. For the flow spins, start point of RF excitations in the initial slice was individually determined based on their velocities such that they arrived at the first following slice at the beginning of acquisition. Results for various start points for the flow spins could be inferred from the simulation results, as described later. The RF excitation profile was assumed to be ideal.

RESULTS

Simulations

The simulation results are shown in Fig. 2. Flow spins had oscillatory magnetization in the initial labeling slice because of RF excitations starting in the middle of data

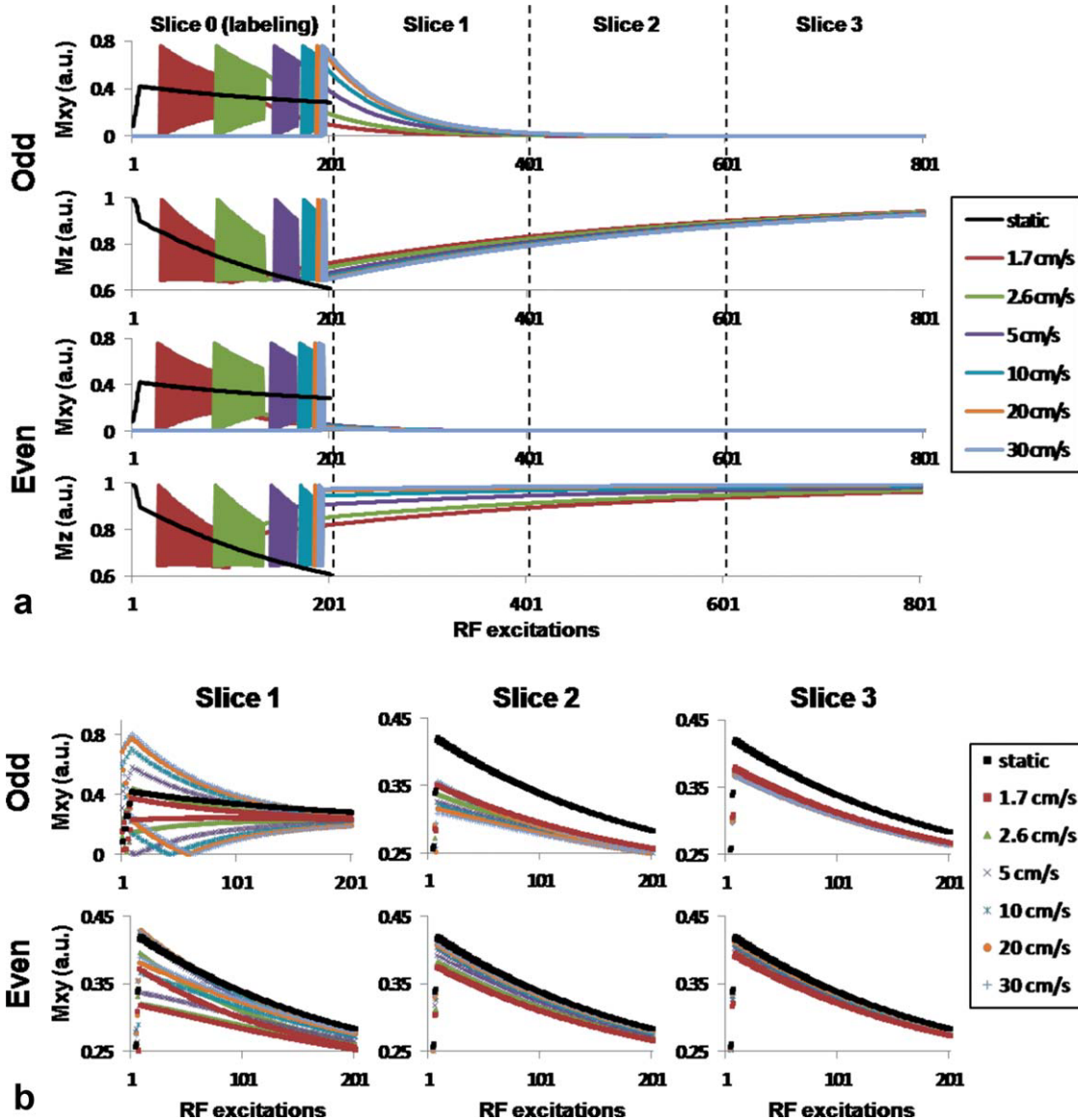


FIG. 2. Simulation results for ALADDIN. **a**: Labeling effects of flow spins with various velocities in sequential 2D bSSFP imaging. The diagrams represent transverse and longitudinal magnetizations of flow spins that experience even or odd numbers of RF excitations in an initial labeling slice (slice 0) and then move through the following slices (slices 1, 2, and 3) with no further RF excitations. The magnetizations at the vertical broken lines represent the initial magnetizations of flow spins in the following slices. **b**: Magnetizations of the flow spins as a function of RF excitations in the three following slices. The results were separately displayed for flow spins with even number and with odd number of RF excitations in the previous labeling slice. Perfusion contrast is the signal differences between the static and flow spins.

acquisition. After moving out of the slice, they showed T_2 -related decay and T_1 -related recovery for transverse and longitudinal magnetizations, respectively, consistent with the previous study (26). Because of the oscillatory characteristics, the flow spins contributed to signals of the following slices in a manner that is different between those with even number and odd number of RF excitations in the initial labeling slice (Fig. 2a). In the following slices, the initial longitudinal magnetization of the flow spins contributed to the perfusion contrast, whereas the initial transverse magnetization led to the oscillatory characteristics even after experiencing the 10 dummy PE steps especially in the first following slice (Fig. 2b).

When signals from the spins with even and odd numbers of excitations in the labeling slice were averaged, overall contributions of the flow spins to perfusion signals did not change significantly with flow velocity in the following slices. During the acquisition of each slice, as the number of RF excitations experienced by the spins increased to 48, 96, 144, and 192, the average magnetization difference (hence, perfusion contrast), respectively, decreased to 79%, 62%, 49%, and 39% of the initial difference (right after the 10 dummy PE steps). In this sense, centric PE order would provide higher perfusion signals than linear PE order. Note that $\sim 40\%$ of the perfusion contrast persists even after all 192 PE steps (when

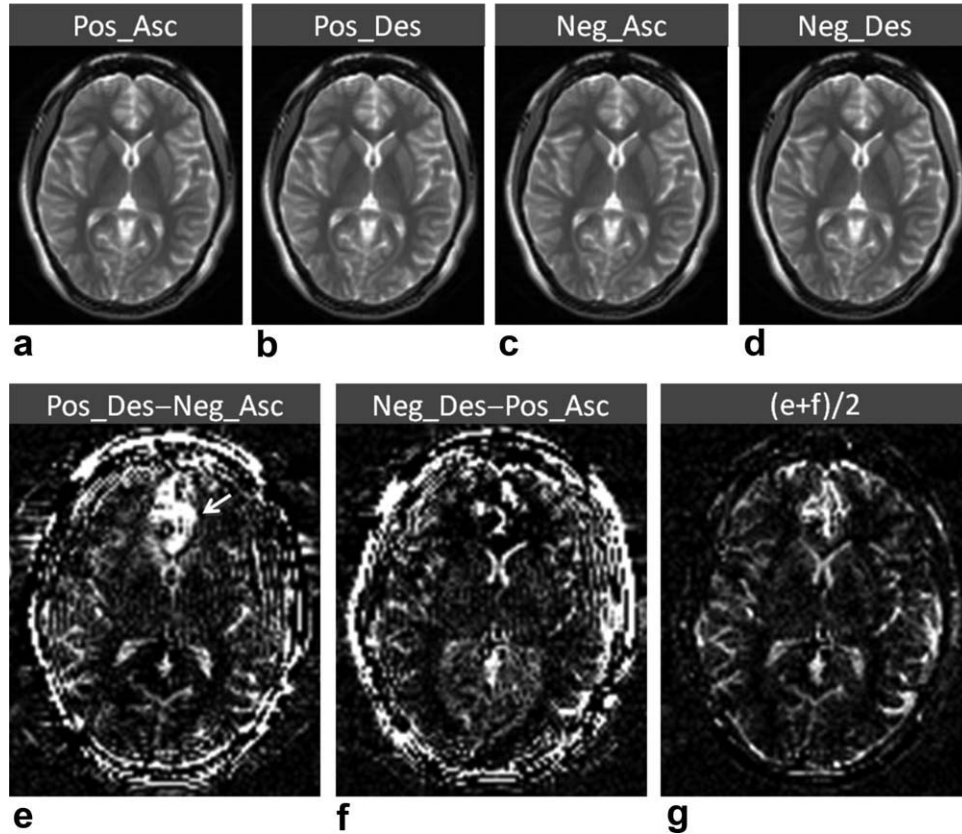


FIG. 3. Demonstration of effects of alternating slice gradient polarities for ALADDIN. Data were acquired with phase oversampling of 100% from one representative subject. **a–d**: Baseline images acquired with positive slice gradient (a,b), negative slice gradient (c,d), and with ascending (a,c) and descending (b,d) orders. **e, f**: Subtraction images between ascending and descending orders with opposite gradient polarities to compensate for MT asymmetry. The two subtraction images still show artifactual signals due to field inhomogeneity and/or gradient imperfection, which is further compensated by averaging the two images as shown in **g**. Note that the image **g** can also be calculated as subtraction between an averaged image from ascending order (a,c) and that from descending order (b,d). Images in **e–g** have the same intensity scale. The arrow in **e** represents the region of cingulate gyrus, where artifacts due to inhomogeneous magnetic fields exist.

phase oversampling was 100%). Flow spins that started RF excitations in the labeling plane at a time different from the simulation would contribute to the following slices in the almost same manner with slightly different T_1 recovery and T_2 decay (hence, initial magnetizations) than the simulation results.

In the other point of view, perfusion signals in the multiple following slices can be viewed as superposition of perfusion signals in a slice from multiple prior labeling planes. When all the velocity components and six prior slices were considered, the perfusion signals from the first, second, third, and fourth prior slices were 44%, 25%, 15%, and 9% of total signals from all the six prior slices. In this sense, >90% of ALADDIN signals in a slice would be from the four prior slices.

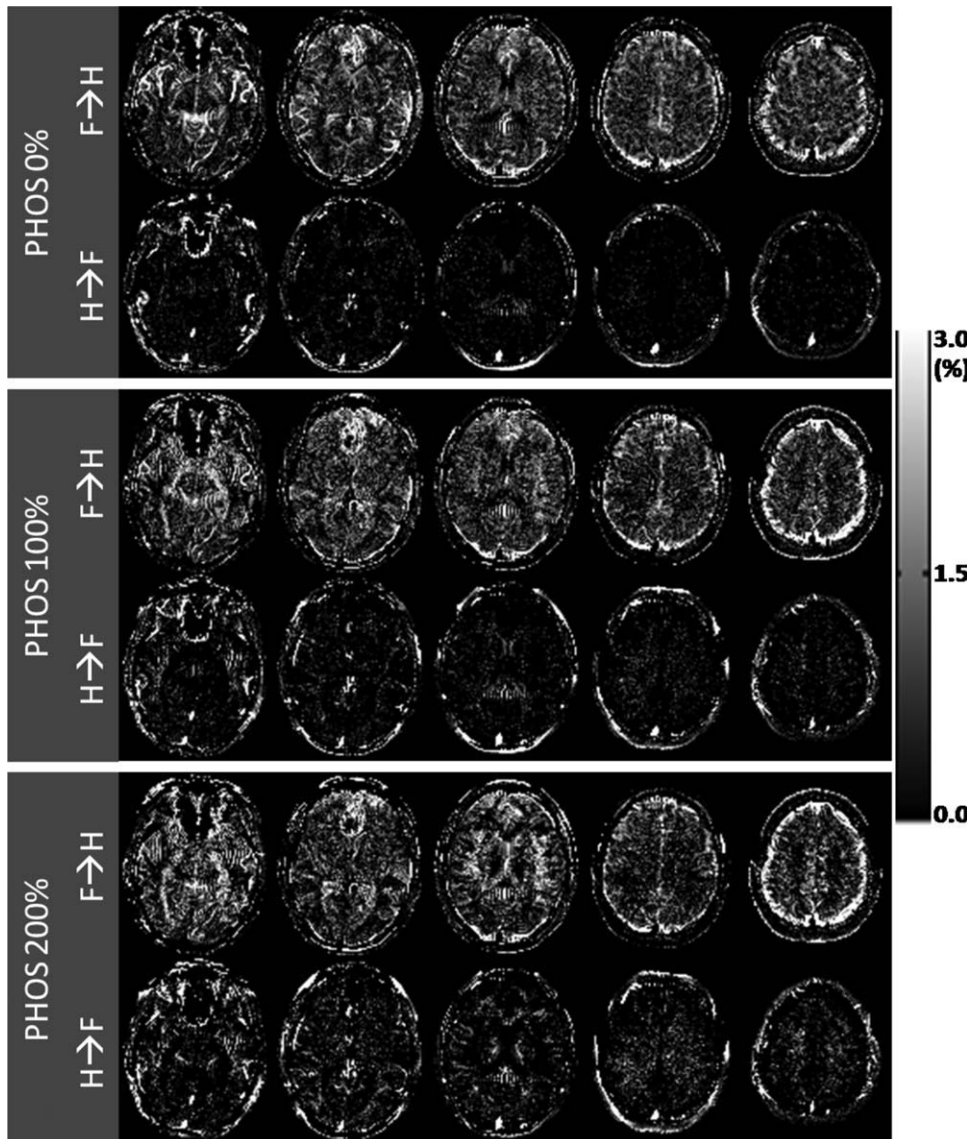
Demonstration of ALADDIN Perfusion-Weighted Imaging

The four different types of ALADDIN acquisitions could compensate effects of MT asymmetry, field inhomogeneity, and gradient imperfection, as demonstrated in Fig. 3. The baseline images of the four types were visually indistinguishable (Figs. 3a–d). The subtraction between the two datasets with opposite gradient polarities (Figs.

3e and f) still showed inhomogeneous signals including bright artifactual signals around the regions of cingulate gyrus (arrow in Fig. 3e), cortical surface regions, and outer regions, presumably due to field inhomogeneity, chemical shift, and/or gradient imperfection. Finally, these artifactual signals could be suppressed by combining the four datasets as shown in Fig. 3g. All the remaining ALADDIN images in this article are shown as combination of the four datasets.

Number of PE Step-Dependent Studies

Depending on phase oversampling, three to five slices on each side of the imaging group were affected by transient MT effects and incomplete T_1 recovery and hence were discarded as dummy slices. In axial images, most GM ALADDIN signals were observed in the perfusion images of “feet → head,” in agreement with conventional methods. When phase oversampling was 0% (number of PE steps = 96), large vascular signals were enhanced (top row in Fig. 4). When phase oversampling increased, these vascular signals were reduced (middle and bottom rows in Fig. 4), consistent with the previous ASL study (6). With phase oversampling, signals in WM regions



3.0 (%)
1.5
0.0

FIG. 4. Number of PE step-dependent experiments for ALADDIN. Images were acquired with phase oversampling of 0, 100, and 200% and corresponding number of PE steps of 96, 192, and 288 (top, middle, and bottom rows, respectively) from the same subject shown in Fig. 3. The perfusion directions are indicated on the left. Total scan time was almost the same (3 min). As number of PE steps increased, large vascular signals were reduced and directional heterogeneity increased especially in WM.

decreased in perfusion images of “feet → head” but increased in those of “head → feet” (Fig. 4), which was reflected in the increased PSC deviation in WM (Table 2). Overall SNR values decreased with phase oversampling (Table 3), presumably due to increased number of RF excitations between the start of acquisition and the K -space center portion. Some big venous vessels such as sagittal sinus vein were detectable as bright spots in the perfusion images of “head → feet”, regardless of phase oversampling (Fig. 4).

Number of Slice- and Gap-Dependent Studies

When phase oversampling was 100%, the ALADDIN signals in the center slice acquired with number of slices = 9 and 3 were about 90% and 20% of those acquired with number of slices = 15 (Tables 2 and 3; Fig. 5). The results showed that 90% of ALADDIN signals in a slice with 192 PE steps were determined by the four prior slices, consistent with the simulation results. The contribution of the first prior slice (20%) was slightly lower than

that from simulation (44%), presumably due to short times for perfusion (as shown with bright vascular signals in Fig. 5c). Flow artifacts in large arteries were consistently observed regardless of number of slices (arrowheads in Fig. 5), while they were not observable in the corresponding baseline images. When phase oversampling was 0% (number of PE steps of 96), about 80% of signals were from the four prior slices (Tables 2 and 3). Note that when phase oversampling was 0 and 100% the time for acquisition of one slice was ~400 and 800 msec, respectively, and the average postlabeling delay from the four prior slices was ~600 and 1200 msec, respectively.

When gap between slices was reduced, ALADDIN signals significantly increased overall and some regions had signals with opposite polarity, especially in WM (top row in Fig. 6a). This directional heterogeneity was demonstrated with increased spatial variance in ALADDIN signals measured within GM and WM (see SD values in Tables 2 and 3). PSC measured in the center slice from the phantom with short T_1 was $0.0 \pm 0.1\%$ for all three gap values and that from the phantom with long T_1 was

Table 2
Mean and SD of Percent Signal Change (PSC_{Mean} and PSC_{SD}) Measured Over GM and WM Regions in ALADDIN Images and PASL Images

Experiment	Variable	GM		WM	
		PSC_{Mean} (%)	PSC_{SD} (%)	PSC_{Mean} (%)	PSC_{SD} (%)
Labeling efficiency	PHOS 0%	1.0 ± 0.1	1.8 ± 0.4	0.5 ± 0.1	0.8 ± 0.0
	PHOS 100%	1.0 ± 0.1	1.9 ± 0.3	0.4 ± 0.1	0.9 ± 0.1
	PHOS 200%	0.7 ± 0.2	1.9 ± 0.2	0.3 ± 0.1	1.1 ± 0.1
No. of labeling planes with PHOS 0%	# slice 15	0.9 ± 0.1	1.6 ± 0.5	0.5 ± 0.0	0.8 ± 0.0
	# slice 9	0.7 ± 0.1	1.5 ± 0.5	0.3 ± 0.2	0.8 ± 0.0
	# slice 3	0.2 ± 0.0	1.0 ± 0.2	0.0 ± 0.0	0.6 ± 0.0
No. of labeling planes with PHOS 100%	# slice 15	1.1 ± 0.1	2.0 ± 0.2	0.5 ± 0.0	0.9 ± 0.1
	# slice 9	1.0 ± 0.1	2.0 ± 0.1	0.6 ± 0.3	0.9 ± 0.1
	# slice 3	0.2 ± 0.1	1.4 ± 0.1	0.0 ± 0.2	0.8 ± 0.0
Flow velocities with PHOS 0%	Gap 140%	0.9 ± 0.1	1.6 ± 0.5	0.5 ± 0.0	0.8 ± 0.0
	Gap 80%	1.2 ± 0.1	1.9 ± 0.4	0.5 ± 0.0	1.2 ± 0.3
	Gap 20%	1.4 ± 0.2	3.2 ± 0.4	0.6 ± 0.7	3.1 ± 0.8
Flow velocities with PHOS 100%	Gap 140%	1.1 ± 0.1	2.0 ± 0.2	0.5 ± 0.0	0.9 ± 0.1
	Gap 80%	1.2 ± 0.2	2.4 ± 0.1	0.7 ± 0.4	1.1 ± 0.4
	Gap 20%	1.6 ± 0.4	4.6 ± 0.5	0.7 ± 0.7	3.0 ± 1.2
Postlabeling delay with centric PE order	PID 200 msec	1.5 ± 0.2	2.1 ± 0.4	0.2 ± 0.2	1.1 ± 0.0
	PID 700 msec	0.8 ± 0.2	1.5 ± 0.3	0.1 ± 0.3	0.8 ± 0.0
	PID 1200 msec	0.4 ± 0.1	1.4 ± 0.6	0.1 ± 0.1	0.7 ± 0.1
PASL ($N = 6$)		0.4 ± 0.1	0.2 ± 0.0	0.1 ± 0.1	0.1 ± 0.1

PHOS represent phase oversampling. All the values are measured from the center slice of each imaging group and are given as mean \pm SD across subjects.

0.1 ± 0.4 , 0.1 ± 0.2 , and $0.0 \pm 0.2\%$ for gap value of 140%, 80%, and 20%, respectively, of slice thickness (middle and bottom rows in Fig. 6a). The excitation profile of the RF pulse indicated that crosstalk effects might contribute to the ALADDIN signals except the scans with 140% gap (7 mm) (Fig. 6b). However, the ALADDIN signals in phantom images were mostly suppressed and

some residual signals in the phantom with longer T_1 were not dependent on gap (bottom row in Fig. 6a), in contrast to the in vivo data (top row in Fig. 6a). These results imply that crosstalk effects of static spins might not be the major source of the increased ALADDIN signals with the reduced gap, although the differences in frequency distributions between the phantoms and the

Table 3
Signal Mean and SD to Noise Ratio (SNR_{Mean} and SNR_{SD}) Measured Over GM and WM Regions in ALADDIN Images and in PASL Images

Experiment	Variable	GM		WM	
		SNR_{Mean}	SNR_{SD}	SNR_{Mean}	SNR_{SD}
Labeling efficiency	PHOS 0%	4.8 ± 0.9	10.8 ± 3.6	1.9 ± 0.4	3.0 ± 0.6
	PHOS 100%	3.9 ± 0.7	9.8 ± 2.8	1.2 ± 0.3	2.5 ± 0.2
	PHOS 200%	2.7 ± 0.6	8.8 ± 2.0	0.7 ± 0.3	2.7 ± 0.4
No. of labeling planes with HOS 0%	# slice 15	4.2 ± 0.6	8.7 ± 3.2	1.7 ± 0.1	2.4 ± 0.4
	# slice 9	3.3 ± 0.6	8.3 ± 3.1	0.9 ± 0.5	2.8 ± 0.2
	# slice 3	1.2 ± 0.1	5.3 ± 1.3	0.0 ± 0.2	2.3 ± 0.2
No. of labeling planes with PHOS 100%	# slice 15	4.4 ± 0.7	11.7 ± 1.8	1.3 ± 0.2	2.6 ± 0.2
	# slice 9	3.8 ± 0.4	10.4 ± 0.8	1.2 ± 0.3	2.4 ± 0.2
	# slice 3	0.8 ± 1.2	7.6 ± 1.0	-0.2 ± 0.1	2.3 ± 0.2
Flow velocities with PHOS 0%	Gap 140%	4.2 ± 0.6	8.7 ± 3.2	1.7 ± 0.1	2.4 ± 0.4
	Gap 80%	5.2 ± 0.3	9.8 ± 2.4	1.6 ± 0.1	3.2 ± 0.4
	Gap 20%	5.6 ± 0.7	14.4 ± 2.5	1.4 ± 1.7	6.7 ± 1.4
Flow velocities with PHOS 100%	Gap 140%	4.4 ± 0.7	11.7 ± 1.8	1.3 ± 0.2	2.6 ± 0.2
	Gap 80%	4.5 ± 0.7	11.5 ± 1.1	1.3 ± 0.3	3.7 ± 0.4
	Gap 20%	5.2 ± 1.2	15.9 ± 0.9	0.9 ± 0.3	8.9 ± 1.1
Postlabeling delay with centric PE order	PID 200 msec	7.2 ± 0.9	9.9 ± 1.2	0.5 ± 0.8	3.7 ± 0.2
	PID 700 msec	4.3 ± 0.9	7.9 ± 1.4	0.5 ± 1.2	3.4 ± 0.3
	PID 1200 msec	2.7 ± 0.6	7.9 ± 3.3	0.6 ± 0.4	3.2 ± 0.5
PASL ($N = 6$)		7.2 ± 1.9	3.8 ± 0.5	2.7 ± 1.3	2.7 ± 1.3
		(14.4 ± 3.9)	(7.6 ± 1.0)	(5.4 ± 2.7)	(5.4 ± 2.7)

PHOS represent phase oversampling. SNR values for PASL were converted to the values with the same scan resolution as ALADDIN, and the parentheses represent the original SNR values before the conversion. All the values are measured from the center slice of each imaging group and are given as mean \pm SD across subjects.

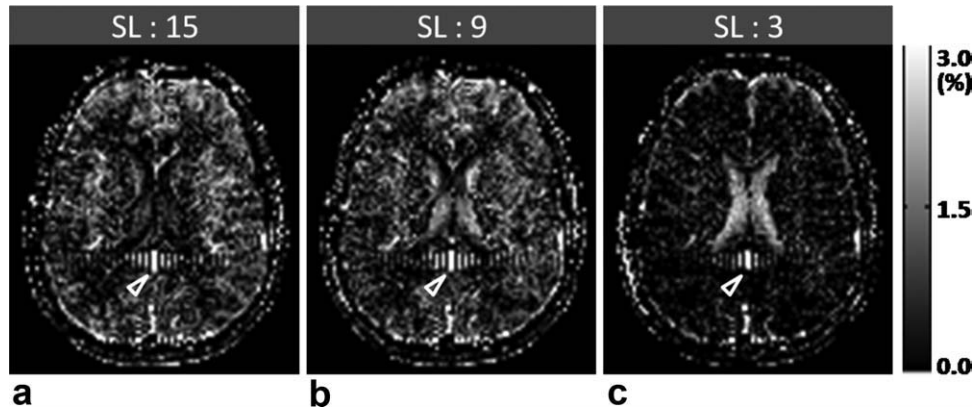


FIG. 5. Number of slice-dependent experiments for ALADDIN. Data were acquired with phase oversampling of 100% from a subject different from Figs. 3 and 4. "SL" represents total number of slices and the images are from the center of each imaging group. Perfusion signals were relatively preserved between SL of 15 (a) and 9 (b), but was significantly reduced when SL = 3 (c). Arrowheads represent flow artifacts. See text for details.

in vivo brains were taken into account. Nonetheless, all the other studies were performed with gap of 140% of slice thickness to ensure no crosstalk effect.

Centric PE Order for ALADDIN

PSC and SNR were higher in datasets with centric PE order (PID = 200 msec) than linear PE order (Fig. 7a and Tables 2 and 3), consistent with the simulation result. Flow artifacts were also reduced in the centric PE order (arrowheads in Fig. 7a). However, ALADDIN with the

centric PE order was not stable in two out of the five subjects, where signal asymmetry between hemispheres or signal void was observed in four to five slices out of nine slices (not including dummy slices). Also the centric PE order showed wave-like artifacts around regions of large arteries. Linear PE order showed much more stable signal performance with fewer dummy PE steps in overall brain regions, despite the lower sensitivity.

As PID increased, perfusion signal decreased throughout GM regions (Fig. 7b and Tables 2 and 3). When PID = 700 msec, signals with opposite polarity increased in

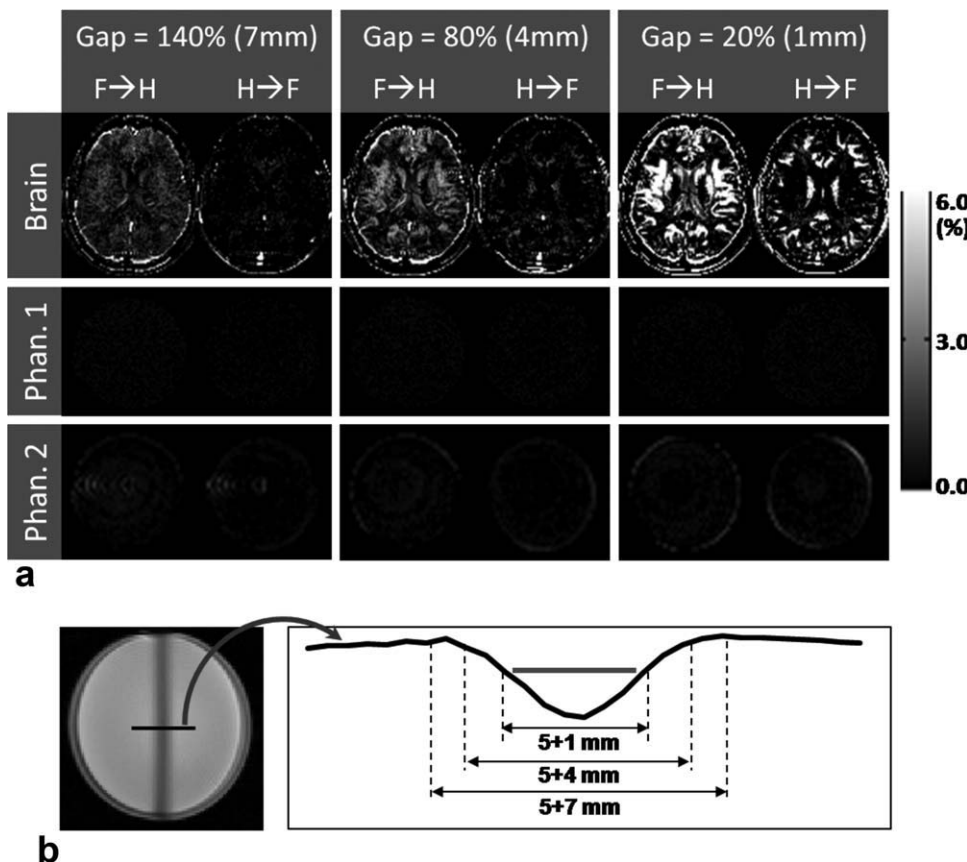
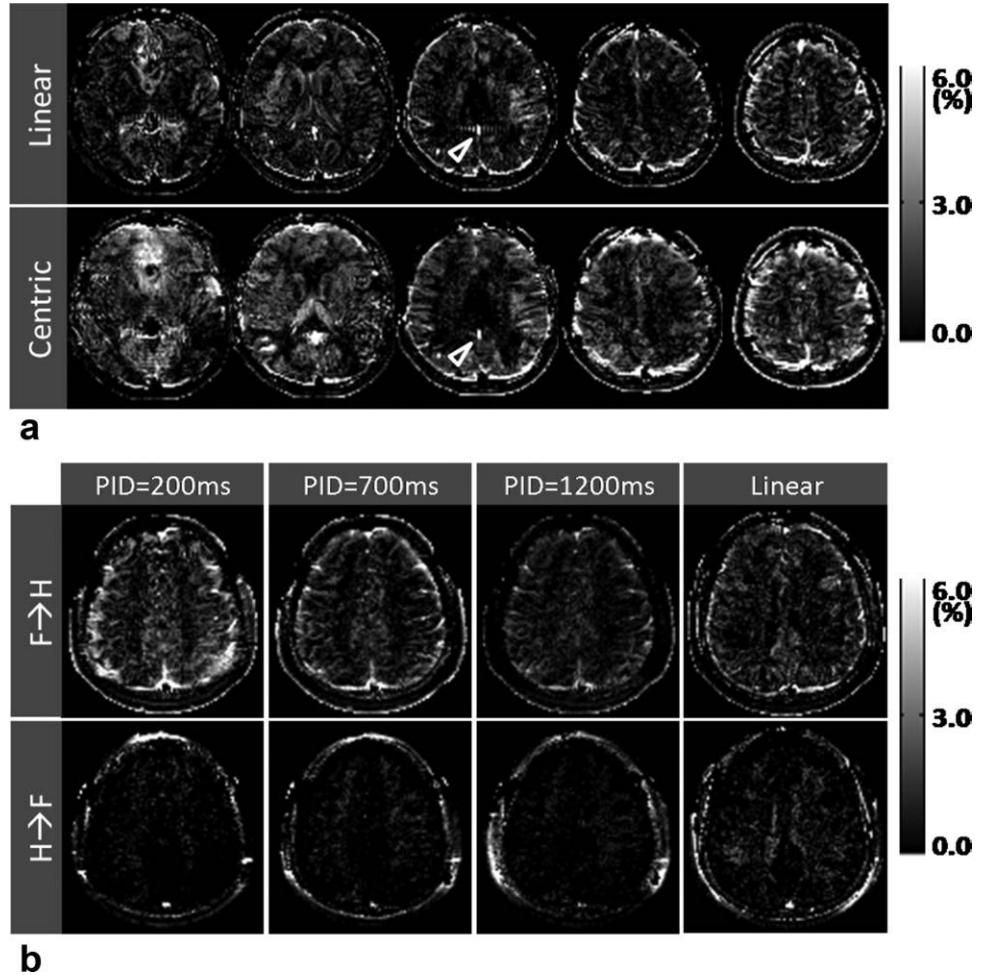


FIG. 6. ALADDIN signals as a function of gap. a: Gap-dependent experiments for ALADDIN performed for in vivo (top row) and two uniform phantoms: one with T_1 and T_2 of 110 and 75 msec (middle row) and the other with T_1 and T_2 of 4000 and 500 msec (bottom row). The center slice of each imaging group acquired with gap of 140% (7 mm), 80% (4 mm), and 20% (1 mm) is shown in left, middle, and right columns, respectively. All the datasets were acquired with phase oversampling of 100%. The in vivo data (a) were from a subject different from Figs. 3–5. b: Experimentally measured excitation profile of the RF pulse. Gray bar above the profile represents the actual thickness (5 mm) and broken lines represent boundary of spatial regions in consideration of the three gap values.

FIG. 7. Centric PE order for ALADDIN. **a**: Data acquired with linear (top) and centric (bottom) PE orders with phase oversampling of 200% from a subject different from Figs. 3–6. Centric PE order shows higher signals than linear PE order. Arrowheads represent flow artifacts. **b**: Images acquired with various interslice PID times for centric PE order and an image acquired with linear PE order from a subject different from Figs. 3–6 and 7a. Note the scale is different from the previous in vivo images shown in Figs. 3–5.



some regions, especially in WM, and further increased in the images with linear PE order (Fig. 7b). These observations were visually consistent in the three subjects with stable ALADDIN signals, although the effects were not big enough to be reflected in the quantifications (Tables 2 and 3).

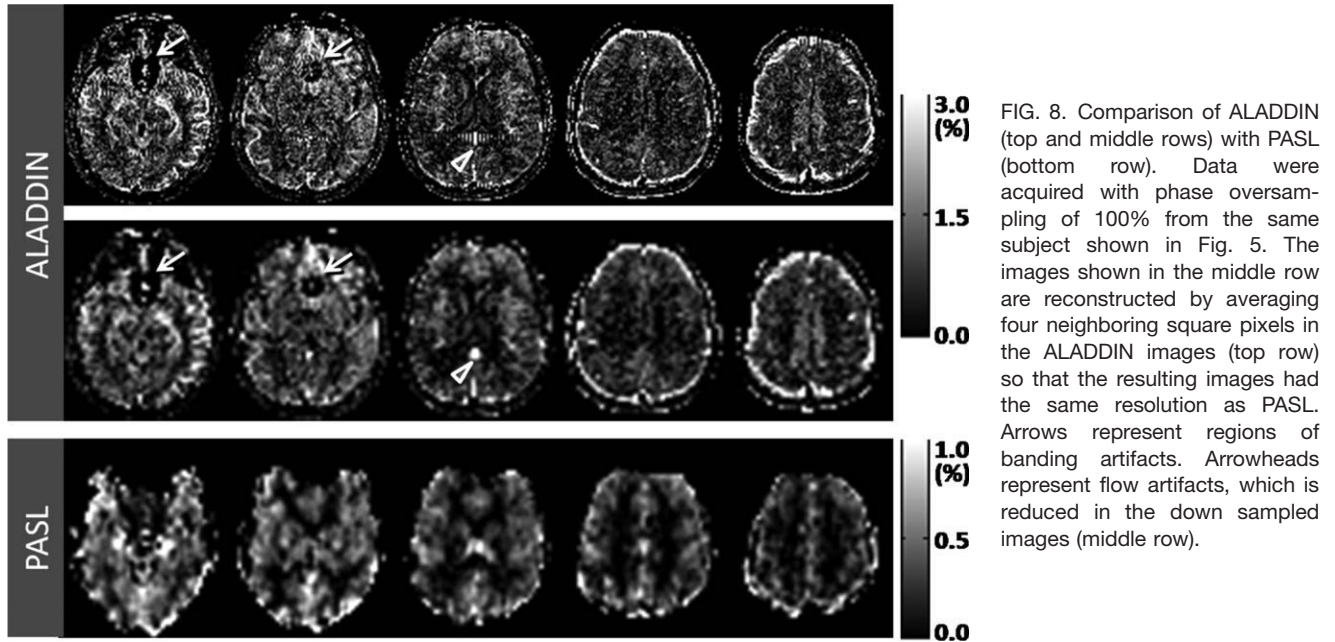
Comparison of ALADDIN with PASL

The PSC from ALADDIN were higher than that from PASL by 2.5 times or more (Table 2). The PSC value of PASL in GM is relatively consistent with that from the previous study (12). Mean SNR (SNR_{Mean}) of ALADDIN was mostly lower than that of PASL, except the centric PE order with PID = 200 msec (Table 3). However, SD of SNR (SNR_{SD}) of ALADDIN was mostly higher than both SNR_{Mean} and SNR_{SD} of PASL (Table 3). The high signal heterogeneity within GM and WM regions of ALADDIN might represent the perfusion directional heterogeneity within the regions. Although SNR of PASL might be increased by $\sim 15\%$ by reducing TR from 4 to 3 sec and increasing number of averages accordingly, the trend for SNR would be similar. To visually compare the perfusion images from ALADDIN and PASL (top and bottom rows in Fig. 8) in the same resolution, four neighboring square pixels in ALADDIN images were averaged (middle row in Fig. 8). In terms of GM/WM contrast, the

down sampled ALADDIN images and the PASL images were visually similar. The EPI-based PASL images showed spatial distortion and signal dropouts due to susceptibility effects, whereas ALADDIN perfusion-weighted images showed virtually no distinguishable spatial distortion but signal voids in the regions of banding artifacts (arrows in Fig. 8). Flow artifacts in ALADDIN were suppressed in the down sampled images (arrowheads in Fig. 8). Also rim-like bright signals were observed in ALADDIN images in the distal brain regions (two rightmost images of top and middle rows in Fig. 8). CSF signals distinguishable from the baseline images were bright in some regions but not discernible or dark in other regions of ALADDIN images.

Sagittal and Coronal ALADDIN Perfusion-Weighted Images and MT Asymmetry Signals

There was a change in perfusion direction in the sagittal and coronal ALADDIN images (Figs. 9 and 10). Perfusion in GM was mostly from brain center to lateral, anterior, or posterior, as expected. Perfusion in some WM regions was opposite, i.e., from lateral, anterior, or posterior to brain center. These observations were consistent for all the six subjects with phase oversampling of 0 and 100%. Large blood vessels not discernible in the corresponding baseline images were clearly detectable throughout brain



regions in images acquired with phase oversampling of 0% ($N = 3$) but were reduced in images acquired with phase oversampling of 100% ($N = 3$; Figs. 9 and 10), consistent with the axial imaging (Fig. 4). Perfusion in GM and WM of cerebellum was clearly detectable in the sagittal and coronal images with the same perfusion direction as those in the cerebral regions (Figs. 9 and 10).

In contrast with the directional changes in the sagittal and coronal ALADDIN perfusion-weighted images (Figs. 9 and 10), the polarity of MT asymmetry signals along all three scan directions did not change throughout brain regions. The flow artifacts observed in ALADDIN axial perfusion-weighted images (Figs. 5, 7a, and 8) were also not observable in the MT asymmetry signals.

DISCUSSION AND CONCLUSION

ALADDIN is a new perfusion-weighted imaging technique that requires no separated spin preparation. ALADDIN has a few more distinctive characteristics compared with the previous ASL methods. First, ALADDIN has high sensitivity to tagged spins from both slow- (1–10 cm/sec) and fast-moving (>10 cm/sec) blood. The reduced gap values enable to label blood vessels with velocity even <1 cm/sec and to further reduce T_1 recovery of labeled blood spins. Sensitivity of bSSFP to longitudinal magnetization differences and presence of multiple labeling planes proximal to imaging planes contribute to the perfusion contrast of ALADDIN. All these characteristics of ALADDIN compensated the lower labeling efficiency and provided us with high-resolution multisectional perfusion-weighted images

FIG. 9. Sagittal ALADDIN perfusion images acquired with phase oversampling of 100% from the same subject shown in Fig. 6a. The upper images are those representing perfusion from right to left and the lower images from left to right. Both the upper and lower images are continuously displayed from right (R) to left (L). Perfusion in most GM region is from medial to lateral, whereas in some WM regions it is from lateral to medial. Total number of slices including the dummy slices on each side was 19 and total scan time was 4.6 min.

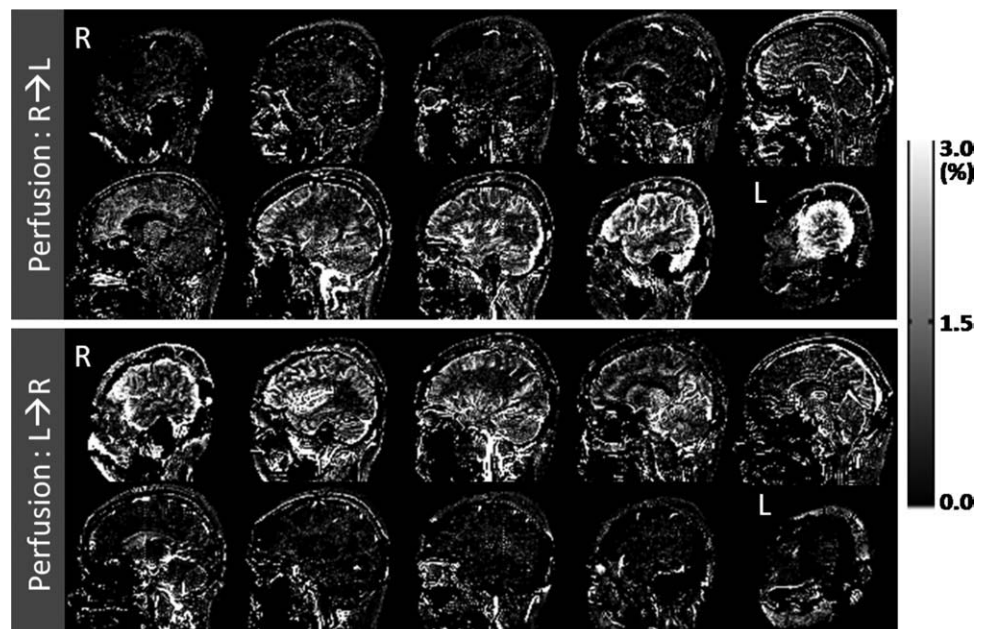
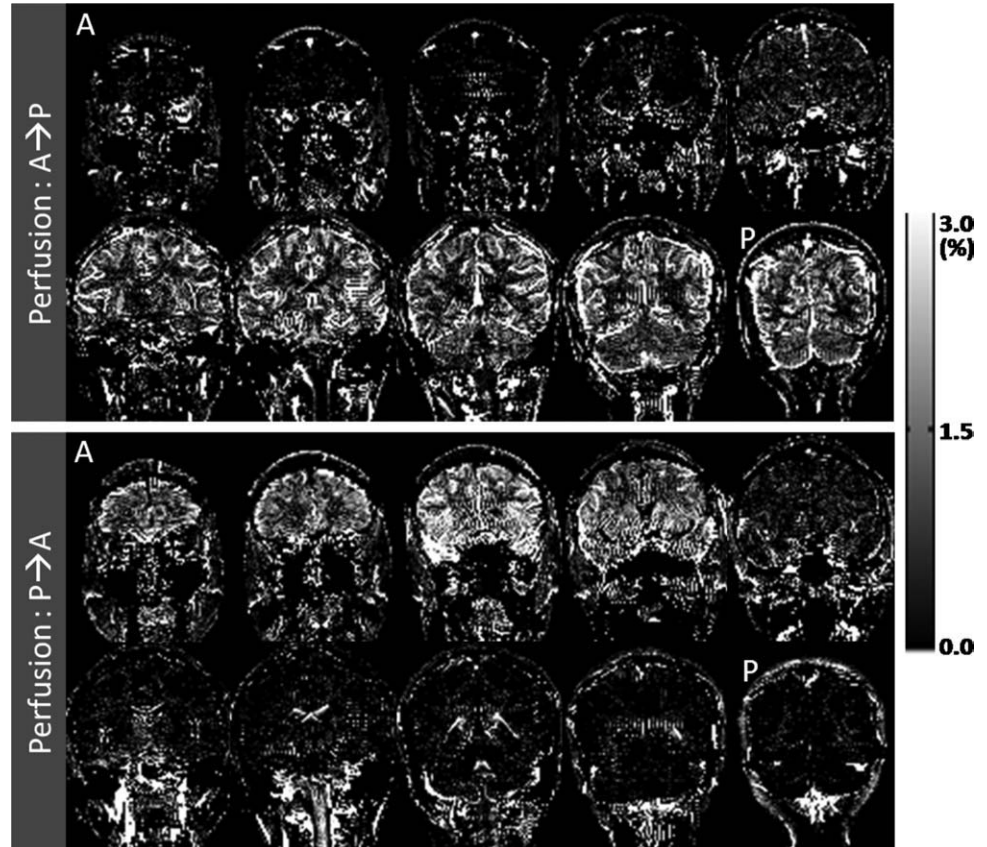


FIG. 10. Coronal ALADDIN perfusion images acquired with phase oversampling of 100% from the same subject shown in Fig. 7a. The upper images are those representing perfusion from anterior to posterior and the lower images from posterior to anterior. Both the upper and lower images are continuously displayed from anterior (A) to posterior (P). Perfusion in most GM region is from center to anterior or posterior, whereas in some WM regions it is opposite. Total number of slices including the dummy slices on each side was 19 and total scan time was 3.6 min.



in ~ 3 min. Second, we can acquire directional perfusion information with multiple slices, which has been uncommon in the previous methods. Images with different scan directions in ALADDIN provide completely differential perfusion information because of changes in labeling direction, as shown in the sagittal and coronal ALADDIN images. Third, it is possible to investigate perfusion characteristics in regions with long blood transit time (e.g., WM) including its directionality because of short distance between labeling and imaging planes. Fourth, there is virtually no limitation in in-plane scan resolution or number of slices, while these are limited by a certain time window in the previous ASL methods.

RF excitation in bSSFP corresponds to the control part of pCASL (12,13). However, the contrast mechanism of ALADDIN is completely different from that of pCASL. The pCASL method uses flow-driven adiabatic inversion for labeling and partial saturation from alternating RF excitation phases for control. Short TR (~ 1 msec) is essential for pCASL to minimize aliasing in labeling slices for flow spins. The pCASL technique is likely sensitive to fast-moving blood (>10 cm/sec) because of relatively long distance between labeling and imaging planes. ALADDIN uses partial saturation of flow spins for labeling and no saturation of flow spins for control. This partial saturation is likely less sensitive to TR values. Presence of multiple labeling planes proximal to imaging planes makes ALADDIN sensitive to both slow- and fast-moving blood. In terms of postlabeling delay, ALADDIN is a mixture of ~ 0 , 800, 1600, and 2400 msec when

phase oversampling was 100%, whereas pCASL has only one postlabeling delay time of ~ 1500 msec. In pCASL, the flow-driven adiabatic inversion is achieved in the presence of an average nonzero gradient along slice-select direction (12,13), whereas the average gradient along all three directions is zero in bSSFP. Therefore, fast low-angle shot sequence with high flip angle may be a good alternative to bSSFP for ALADDIN in terms of labeling efficiency.

Wong et al. (27) proposed a technique called velocity-selective ASL (VSASL) and there are similarities and differences between VSASL and ALADDIN. VSASL labels blood spins within a selected velocity range in a spatially nonselective way, whereas ALADDIN labels blood spins with a minimum velocity determined by interslice gap in a spatially selective way. VSASL can provide directional perfusion information based on changes in direction of velocity encoding gradient (28). ALADDIN also provides directional perfusion information but based on changes in labeling direction. Therefore, ALADDIN may provide directionality of local blood supply in each voxel that is different from the VSASL-based method (28).

There are several factors that potentially contribute to higher PSC in ALADDIN. Sensitivity to blood in a wider velocity range (especially slowly moving blood) might increase PSC. As pCASL showed $\sim 60\%$ higher PSC than PASL (12), the semicontinuous labeling nature of ALADDIN might contribute to the higher PSC to a certain degree. Also centric PE order showed much higher

PSC than linear PE order in ALADDIN; hence, relatively short postlabeling delay of ALADDIN compared with PASL might also contribute to the higher PSC.

The transverse magnetization from the flow spins caused oscillation in the slice of interest (Fig. 2b); hence, it potentially caused flow artifacts in the resulting images. Because of the oscillation, the artifacts would be different between centric and linear PE orders, consistent with the results in Fig. 7a. As the artifacts were observable in neither the corresponding baseline images nor MT asymmetry signals, they would not be from imperfect flow compensation along the PE direction.

Inflow effects also contribute to ALADDIN signals. Most labeled spins with inflow effects in the imaging plane are presumably from the first prior slice because of the longer postlabeling delay from the slices acquired earlier. Because signals from the first prior slice were ~20% of total signals, contributions of the inflow effects to ALADDIN signals would be <20%.

Venous blood can be labeled and detected in ALADDIN. Contributions of labeled venous blood to ALADDIN signals in large veins were visually distinguishable (images of "head → feet" in Fig. 4), because venous blood drains into larger vessels rather than perfusing into tissue. Labeled venous blood in smaller veins might reduce ALADDIN signals through partial volume effects, because its flow direction is opposite to that of arterial blood.

ALADDIN is likely more sensitive to CSF flow than any other ASL techniques because of short distance between labeling and imaging planes. ALADDIN signals in some large CSF regions were affected by CSF flow. The rim-like bright signals in the distal brain regions (Fig. 8) could be from CSF or large surface blood vessels. However, the polarity of ALADDIN signals in most GM regions along all the three imaging directions matches blood perfusion direction (rather than net CSF flow direction). Also peak CSF velocity in cerebral aqueduct ranges 3–9 cm/sec, but the averaged velocity within a cycle of 650 msec duration ranges 0.1–1 cm/sec because of bidirectional movement (29). Therefore, contributions of smaller CSF regions to ALADDIN signals may not be significant. Acquisition of ALADDIN signals free of CSF contributions may be possible with inversion recovery.

In this article, signal sources of ALADDIN has been investigated in an indirect way by analyzing all the potential signal sources other than perfusion, i.e., transient MT, MT asymmetry, interslice crosstalk, magnetic field inhomogeneity, venous blood flow, and CSF flow. As mentioned above, the contributions of venous blood flow and CSF flow would be visually distinguishable or relatively small. In this study, the polarity of MT asymmetry signal that is not dependent on scan direction supports good separation of ALADDIN perfusion signals from MT asymmetry signals.

As the number of dummy PE steps decreased, the stability of centric PE order became worse (data not shown). This result implies that the instability of centric PE order is related to the unstable initial magnetization period, during which signal variations over repetitions may also be high. Centric PE order may be more susceptible to the instability, as the *K*-space center portion rather than the

edge portion is acquired during the unstable initial period. To satisfy both the sensitivity of centric PE order and the stability of linear PE order, ALADDIN datasets may be acquired with (i) partial Fourier, where the *K*-space center lines are acquired at an earlier time point or (ii) a specific *K*-space reordering scheme, where the *K*-space center part is acquired earlier than the *K*-space edge part while maintaining linear PE order in each part (30).

The WM ALADDIN signals with opposite polarity were enhanced in dataset acquired with centric PE order and effective PID of ~700 msec and in dataset acquired with linear PE order and phase oversampling of 200% (Fig. 7b). Note that the *K*-space center lines were acquired ~600 msec after the start of acquisition for the linear PE order. Based on these results, perfusion in WM is likely related to labeling duration and blood transit time (postlabeling delay of ~600 msec when gap was 7 mm). Further study is necessary to better understand the characteristics of WM perfusion in terms of perfusion direction and the delayed enhancement.

Disadvantage of ALADDIN is low temporal resolution. The technique requires combination of the four datasets and dummy slices on each side of the imaging group. The former may make the technique susceptible to subject motion or physiological noise. Increased delay time between repetitions may be in favor of reducing the number of dummy slices because of more complete recovery of magnetization in edge slices. Also banding artifacts in bSSFP are problematic but are easier to identify than distortion and susceptibility artifacts in EPI and may be removable with multiple phase cycling approaches (31–33). Quantitative prediction of signal change in ALADDIN requires the knowledge of blood velocity distributions; hence, more complicated physiological and mathematical modeling may be needed. The modeling would be an important step toward estimation of absolute blood perfusion in ALADDIN.

ALADDIN requires no additional hardware and is easier to implement than any other ASL techniques. In addition to gap, number of PE steps, and PE order mentioned above, there are many other factors that affect ALADDIN perfusion signals such as RF flip angle and duration, TR, slice thickness, and scan resolution, all of which can be further optimized. Based on all these characteristics, ALADDIN is potentially valuable in many clinical, physiological, and neurological studies. Further studies are necessary to confirm signal sources of ALADDIN to investigate directional perfusion information in each voxel, quantify absolute perfusion values in conventional units (ml/100g/min), compare bSSFP with other sequences including fast low-angle shot, and compare optimized sensitivity of ALADDIN with that of continuous ASL (6–11) and pCASL (12–14).

REFERENCES

1. Edelman RR, Siewert B, Darby DG, Thangaraj V, Nobre AC, Mesulam MM, Warach S. Qualitative mapping of cerebral blood flow and functional localization with echo-planar MR imaging and signal targeting with alternating radio frequency. *Radiology* 1994;192:513–520.
2. Kim SG. Quantification of relative cerebral blood flow change by flow-sensitive alternating inversion recovery (FAIR) technique:

- application to functional mapping. *Magn Reson Med* 1995;34:293–301.
3. Kwong KK, Chesler DA, Weisskoff RM, Donahue KM, Davis TL, Ostergaard L, Campbell TA, Rosen BR. MR perfusion studies with T1-weighted echo planar imaging. *Magn Reson Med* 1995;34:878–887.
 4. Wong EC, Buxton RB, Frank LR. Implementation of quantitative perfusion imaging techniques for functional brain mapping using pulsed arterial spin labeling. *NMR Biomed* 1997;10:237–249.
 5. Luh WM, Wong EC, Bandettini PA, Hyde JS. QUIPSS II with thin-slice T1 periodic saturation: a method for improving accuracy of quantitative perfusion imaging using pulsed arterial spin labeling. *Magn Reson Med* 1999;41:1246–1254.
 6. Alsop DC, Detre JA. Reduced transit-time sensitivity in noninvasive magnetic resonance imaging of human cerebral blood flow. *J Cereb Blood Flow Metab* 1996;16:1236–1249.
 7. Alsop DC, Detre JA. Multisection cerebral blood flow MR imaging with continuous arterial spin labeling. *Radiology* 1998;208:410–416.
 8. Detre JA, Leigh JS, Williams DS, Koretsky AP. Perfusion imaging. *Magn Reson Med* 1992;23:37–45.
 9. Pekar J, Jezzard P, Roberts DA, Leigh JS Jr, Frank JA, McLaughlin AC. Perfusion imaging with compensation for asymmetric magnetization transfer effects. *Magn Reson Med* 1996;35:70–79.
 10. Wang J, Zhang Y, Wolf RL, Roc AC, Alsop DC, Detre JA. Amplitude-modulated continuous arterial spin-labeling 3.0-T perfusion MR imaging with a single coil: feasibility study. *Radiology* 2005;235:218–228.
 11. Williams DS, Detre JA, Leigh JS, Koretsky AP. Magnetic resonance imaging of perfusion using spin inversion of arterial water. *Proc Natl Acad Sci USA* 1992;89:212–216.
 12. Wu WC, Fernandez-Seara M, Detre JA, Wehrli FW, Wang J. A theoretical and experimental investigation of the tagging efficiency of pseudocontinuous arterial spin labeling. *Magn Reson Med* 2007;58:1020–1027.
 13. Dai W, Garcia D, de Bazelaire C, Alsop DC. Continuous flow-driven inversion for arterial spin labeling using pulsed radio frequency and gradient fields. *Magn Reson Med* 2008;60:1488–1497.
 14. Wong EC. Vessel-encoded arterial spin-labeling using pseudocontinuous tagging. *Magn Reson Med* 2007;58:1086–1091.
 15. Oppelt A, Graumann R, Barfub H, Fischer W, Hartl W, Schajor W. FISP — a new fast imaging sequence. *Electromedica* 1986;54:15–18.
 16. Scheffler K, Lehnhardt S. Principles and applications of balanced SSFP techniques. *Eur Radiol* 2003;13:2409–2418.
 17. Martirosian P, Klose U, Mader I, Schick F. FAIR true-FISP perfusion imaging of the kidneys. *Magn Reson Med* 2004;51:353–361.
 18. Boss A, Martirosian P, Klose U, Nagele T, Claussen CD, Schick F. FAIR-TrueFISP imaging of cerebral perfusion in areas of high magnetic susceptibility differences at 1.5 and 3 Tesla. *J Magn Reson Imaging* 2007;25:924–931.
 19. Williams DM, Meyer CR, Schreiner RJ. Flow effects in multislice, spin-echo magnetic resonance imaging. Model, experimental verification, and clinical examples. *Invest Radiol* 1987;22:642–650.
 20. Dixon WT, Engels H, Castillo M, Sardashti M. Incidental magnetization transfer contrast in standard multislice imaging. *Magn Reson Imaging* 1990;8:417–422.
 21. Melki PS, Mulkern RV. Magnetization transfer effects in multislice RARE sequences. *Magn Reson Med* 1992;24:189–195.
 22. Santyr GE. Magnetization transfer effects in multislice MR imaging. *Magn Reson Imaging* 1993;11:521–532.
 23. Zhou J, Payen JF, Wilson DA, Traystman RJ, van Zijl PC. Using the amide proton signals of intracellular proteins and peptides to detect pH effects in MRI. *Nat Med* 2003;9:1085–1090.
 24. Hua J, Jones CK, Blakeley J, Smith SA, van Zijl PC, Zhou J. Quantitative description of the asymmetry in magnetization transfer effects around the water resonance in the human brain. *Magn Reson Med* 2007;58:786–793.
 25. Friston KJ, Ashburner J, Poline JB, Frith CD, Heather JD, Frackowiak RSJ. Spatial registration and normalization of images. *Hum Brain Mapp* 1995;2:165–189.
 26. Markl M, Alley MT, Elkins CJ, Pelc NJ. Flow effects in balanced steady state free precession imaging. *Magn Reson Med* 2003;50:892–903.
 27. Wong EC, Cronin M, Wu WC, Inglis B, Frank LR, Liu TT. Velocity-selective arterial spin labeling. *Magn Reson Med* 2006;55:1334–1341.
 28. Frank LR, Lu K, Wong EC. Perfusion tensor imaging. *Magn Reson Med* 2008;60:1284–1291.
 29. Unal O, Kartum A, Avcu S, Etlik O, Arslan H, Bora A. Cine phase-contrast MRI evaluation of normal aqueductal cerebrospinal fluid flow according to sex and age. *Diagn Interv Radiol* 2009;15:227–231.
 30. Park SH, Moon CH, Bae KT. Compatible dual-echo arteriovenography (CODEA) using an echo-specific K-space reordering scheme. *Magn Reson Med* 2009;61:767–774.
 31. Bangerter NK, Hargreaves BA, Vasanawala SS, Pauly JM, Gold GE, Nishimura DG. Analysis of multiple-acquisition SSFP. *Magn Reson Med* 2004;51:1038–1047.
 32. Elliott AM, Bernstein MA, Ward HA, Lane J, Witte RJ. Nonlinear averaging reconstruction method for phase-cycle SSFP. *Magn Reson Imaging* 2007;25:359–364.
 33. Jung KJ. Synthesis methods of multiple phase-cycled SSFP images to reduce the band artifact and noise more reliably. *Magn Reson Imaging* 2010;28:103–118.